JOURNAL OF Materials CHEMISTRY

Distribution of Mn^{3+} and Mn^{4+} species between octahedral and square pyramidal sites in $Bi_2Mn_4O_{10}$-type structure

Ninh Nguyen,* Magah Legrain, Annie Ducouret and Bernard Raveau

Laboratoire CRISMAT, UMR 6508 associée au CNRS, ISMRA et Université de Caen 6, Boulevard du Maréchal Juin, 14050 CAEN Cedex, France. E-mail: nguyen@crismat.ismra.fr

Received 19th October 1998, Accepted 1st December 1998

The cationic distribution in the iron substituted manganites $Bi_2Mn_{4-x}Fe_xO_{10}$ ($0 \leqslant x \leqslant 1$) has been investigated combining X-ray powder diffraction (XRPD), magnetic susceptibility measurements and ^{57}Fe Mössbauer spectroscopy. Iron is at the trivalent state and exhibits, like Mn^{3+} the high spin configuration. It is shown that Fe^{3+} is distributed over the two sites of the structure, octahedral and square pyramidal, with a preferential occupation of the second one. Consideration of the Mn(Fe)–O distances leads, for $x=1$, to the cationic distribution $Bi_2[Mn_{1.66}^{4+}Fe_{0.34}^{3+}]_O[Mn_{1.00}^{3+}Mn_{0.34}^{4+}Fe_{0.66}^{3+}]_P O_{10}$, showing that Mn^{4+} is also susceptible to sit in the pyramidal site. Magnetic and structural study of the oxides $Bi_2Mn_{4-x}Ti_xO_{10}$ ($0 \leqslant x \leqslant 1$) and $Bi_2Mn_{3.75}Al_{0.25}O_{10}$ suggests that Ti^{4+} and Al^{3+} respectively sit in the octahedral and square pyramidal sites of the structure according to the formulae $Bi_2[Mn_{2-x}^{4+}Ti_x^{4+}]_O[Mn_2^{3+}]_P O_{10}$ and $Bi_2[Mn_2^{4+}]_O[Mn_{1.75}^{3+}Al_{0.25}^{3+}]_P O_{10}$.

Introduction

After the recent discovery of colossal magnetoresistance in mixed valent manganese oxides,[1–5] the problem of the distribution of Mn^{3+} and Mn^{4+} species has been of great interest for the understanding of charge ordering phenomena that appears in those compounds (for a review see ref. 6). In this respect, the $Bi_2Mn_4O_{10}$ structure, first studied by Bertaut *et al.*,[7,8] deserves particular attention, due to the presence of two different sites for manganese, with octahedral and pyramidal coordination. Based on bond length values, and on the Jahn-Teller effect of Mn^{3+}, these authors assigned the octahedral and pyramidal sites to Mn^{4+} and Mn^{3+} species respectively. More recently, Giaquinta and zur Loye[9] synthesized the isostructural oxide $Bi_2Fe_2Mn_2O_{10}$. Their structural refinements from single crystal X-ray data show that Fe^{3+} is in octahedral coordination whereas Mn^{4+} sits in the square pyramidal sites. In order to understand this dramatic different behavior of Mn^{4+} in the presence of Fe^{3+}, we have studied the progressive substitution of Fe^{3+} for Mn^{3+}, combining X-ray powder diffraction (XRPD), Mössbauer spectroscopy and electric field gradient (EFG) calculations. In the present paper we report on the solid solution $Bi_2Mn_{4-x}Fe_xO_{10}$ with $0 \leqslant x \leqslant 1$, showing that Fe^{3+} occupies both sites, octahedral and pyramidal, with a preferential occupancy of the latter. It is also shown that the pyramidal site is preferentially occupied by Mn^{3+} rather than Mn^{4+}. Substitutions of manganese by other cations such as Al^{3+} and Ti^{4+} are also studied.

Experimental

The samples were prepared by solid state reaction of Bi_2O_3, MnO_2 and TiO_2 or M_2O_3 (M = Al, Fe), according to the nominal compositions. The powder oxides intimately ground in an agate mortar are pressed in the form of bars and then placed in alumina crucibles and sealed in evacuated silica tubes, in order to avoid a possible volatilization of bismuth. Different thermal treatments were tested, and the best result was obtained by heating the samples at 850 °C for 24 h, and then slowly cooling to room temperature.

X-Ray powder diffraction patterns were registered using a Philips diffractometer with Cu-Kα radiation. The data were collected by step scanning over an angular range of $10 \leqslant 2\theta \leqslant 90°$ and analyzed with the FULLPROF program.[10]

Magnetic susceptibility was registered with a Faraday balance in the temperature range $80 \leqslant T \leqslant 800$ K. ^{57}Fe Mössbauer spectra were obtained at room temperature using a ^{57}Co/Rh γ-ray source. The source velocity (V) was calibrated with pure iron metal at 300 K as a control material. Spectra were fitted with the MOSFIT program.[11]

Results and discussion

Iron substituted oxides $Bi_2Mn_{4-x}Fe_xO_{10}$

For the above conditions a pure phase was isolated for $0 \leqslant x \leqslant 1$. With our experimental procedure it was not possible to extend the homogeneity up to $x=2$, corresponding to the compound $Bi_2Mn_2Fe_2O_{10}$, prepared previously as single crystals using Bi_2O_3 as a flux.[9]

The XRPD patterns of these phases, registered for $x=0.25$, 0.50, 1 were indexed in an orthorhombic cell close to that previously observed for $Bi_2Mn_4O_{10}$.[7,8] The structure was refined in the space group *Pbam* for $Bi_2Mn_3FeO_{10}$ ($x=1$), supposing a statistical distribution of Mn and Fe over the different sites. An ordered distribution of these elements between the two crystallographic sites did not allow any significant variation of the R factor ($R_i \cong 0.06$) to be detected, in agreement with the very close atomic numbers of these elements. The crystallographic data listed in Table 1 show that the a, b and c parameters increase only slightly as x increases, in agreement with the similar sizes of Fe^{3+} and Mn^{3+}. The atomic coordinates (Table 2) confirm the $Bi_2Mn_4O_{10}$-type framework (Fig. 1) built up of chains of edge-sharing MO_6 octahedra and of edge-sharing MO_5 square pyramids (M = Fe, Mn). These two kinds of chains are corner-shared, forming

Table 1 Cell parameters for $Bi_2Mn_{4-x}M_xO_{10}$ (M = Mn, Ti, Fe, Al); space group *Pbam*, $Z=2$

M	x	a/Å	b/Å	c/Å	V/Å^3
Mn	—	7.556(4)	8.530(2)	5.758(5)	371.12
Ti	0.25	7.569(3)	8.528(4)	5.781(2)	373.15
	0.50	7.581(6)	8.529(5)	5.803(2)	375.21
	1.00	7.612(2)	8.532(2)	5.853(2)	380.12
Fe	0.25	7.550(1)	8.541(1)	5.757(2)	371.24
	0.50	7.552(1)	8.547(2)	5.759(4)	371.73
	1.00	7.558(1)	8.546(1)	5.769(5)	372.62
Al	0.25	7.556(2)	8.526(1)	5.757(4)	370.88

Table 2 Atomic coordinates for $Bi_2Mn_3FeO_{10}$

Atom	Site	x	y	z	B/Å^2
Bi	4g	0.1564(2)	0.1641(2)	0	0.70(1)
Mn, Fe (P)	4h	0.3970(7)	0.3482(9)	0.5	0.61(1)
Mn, Fe (O)	4f	0.5	0	0.2587(12)	0.12(2)
O(1)	4e	0	0	0.2854(14)	1
O(2)	8i	0.3921(11)	0.1959(7)	0.2415(12)	1
O(3)	4h	0.1384(13)	0.4256(11)	0.5	1
O(4)	4g	0.1441(11)	0.4351(13)	0	1

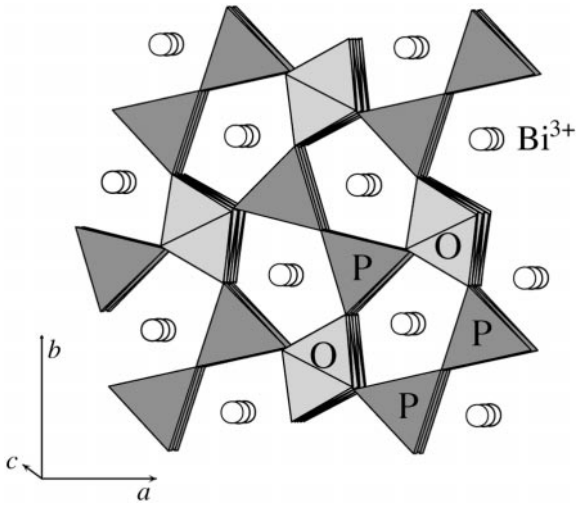

Fig. 1 $Bi_2Mn_4O_{10}$ structure showing the distorted five-membered rings formed by three pyramids and two octahedra.

distorted five-membered rings within which the Bi^{3+} cations are located.

In order to determine the charge and local environment of iron, Mössbauer spectroscopy was performed for the three compounds $Bi_2Mn_3FeO_{10}$ ($x=1$), $Bi_2Mn_{3.5}Fe_{0.5}O_{10}$ ($x=0.50$) and $Bi_2Mn_4O_{10}$ ($x=0$), the latter being doped with 1.5% of ^{57}Fe. The room temperature spectra of these three samples (Fig. 2) show pure electronic quadrupolar interactions. They are fitted with two paramagnetic doublets, even for the $Bi_2Mn_4O_{10}$ doped phase (Table 3). The observed isomer shift values (IS, relative to metallic iron) are characteristic of Fe^{3+} for both sites. The quadrupole splitting, observed in the Mössbauer spectra, corresponds to the asymmetrical part of the electronic hyperfine interaction between the iron nucleus and its surrounding charges (electrons from the iron valence shell and other ions in the crystal). Owing to the spherical symmetry of the $3d^5$ electronic shell of Fe^{3+}, the electric field gradient (EFG) is almost entirely due to the 'lattice' contribution. Thus, the substantial difference between the two experimental values ($\Delta|QS|_{ex}=1.15-0.72=0.43$ mm s^{-1}) clearly indicates a difference in the local symmetry of these two Mössbauer sites.

Thus, in order to attribute the octahedral (O) and pyramidal (P) coordinations to the Mössbauer sites, EFG calculations have been performed for Fe^{3+} in $Bi_2Mn_3FeO_{10}$, using the structural data given in Tables 1 and 2. QS values can then be deduced from the main components V_{XX}, V_{YY}, V_{ZZ} of the EFG 'lattice' tensor by the relation $QS=(1-\gamma_\infty)(eQ/2)V_{ZZ}(1+\eta^{2/3})^{0.5}$ where $(1-\gamma_\infty)$ is the antishielding Sternheimer factor (*ca.* 10.14 for Fe^{3+}),[12] V_{ZZ} is the principal component of the EFG tensor, $\eta=(V_{XX}-V_{YY})/V_{ZZ}$ is the asymmetry parameter ($0\leqslant\eta\leqslant1$, with the convention $|V_{XX}|\leqslant|V_{YY}|\leqslant|V_{ZZ}|$), and Q the quadrupolar moment of the ^{57}Fe nucleus in the excited state $I=3/2$ [$Q\approx0.2$ barn[13] (1 barn $=10^{-28}$ m^2)]. We computed lattice EFG calculations for Fe^{3+} in the O and P sites of the structure successively. In a first step, we only considered the monopolar approximation

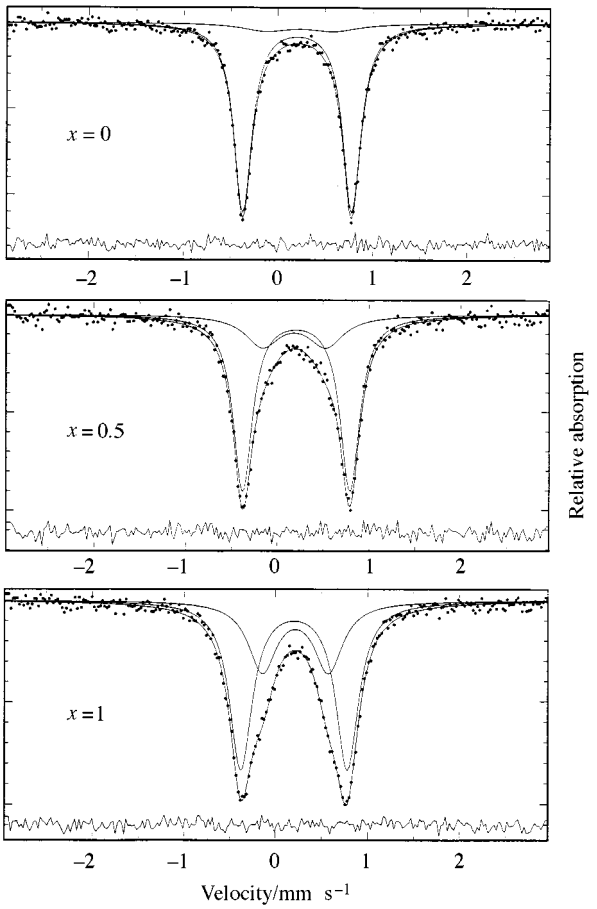

Fig. 2 ^{57}Fe room temperature Mössbauer spectra of $Bi_2Mn_{4-x}Fe_xO_{10}$, $0\leqslant x\leqslant1$.

Table 3 Hyperfine ^{57}Fe Mössbauer parameters at room temperature for $Bi_2Mn_{4-x}Fe_xO_{10}$ ($0\leqslant x\leqslant1$)

x	Site	IS[a]/mm s^{-1}	/QS/$_{ex}$[a]/mm s^{-1}	%[b]
0	P	0.32	1.15	90
	O	0.33	0.72	10
0.5	P	0.32	1.17	76
	O	0.30	0.70	24
1.0	P	0.31	1.15	66
	O	0.32	0.72	34

[a] ±0.2 mm s^{-1}. [b] ±5%.

(charge point model) and the first neighbor oxygens of Fe^{3+}. These calculations show two positive QS values: $QS_O=0.66(1)$ mm s^{-1} [$\eta_O=0.84(1)$] and $QS_P=1.04(1)$ mm s^{-1} [$\eta_P=0.07(1)$]. In spite of the limitations of the calculation, the two values are quite different and allow one to attribute the contribution $|QS|_{ex}=0.72$ mm s^{-1} to Fe^{3+} ion in the octahedral environment (O), and the contribution $|QS|_{ex}=1.15$ mm s^{-1} to Fe^{3+} in the pyramidal environment (P). Note that the difference between QS_P and QS_O [0.38(2) mm s^{-1}] is very close to that observed between the experimental values [0.43(4) mm s^{-1}], which *a posteriori* justifies the monopolar EFG approximation and evidences the major role of the first neighbors in the quadrupolar interaction.

These results show that the distribution of Fe^{3+} in the $Bi_2Mn_{4-x}Fe_xO_{10}$ compounds, prepared here for $0\leqslant x\leqslant1$, differs fundamentally from that obtained previously for $x=2$.[9] One indeed observes that the Fe^{3+} species are distributed over the two sites, pyramidal and octahedral, instead of only one site (octahedral) for the $x=2$ phase. Moreover, it is shown that it is the pyramidal site which is preferentially occupied by Fe^{3+} (Table 3). Nevertheless, it is worth pointing out that

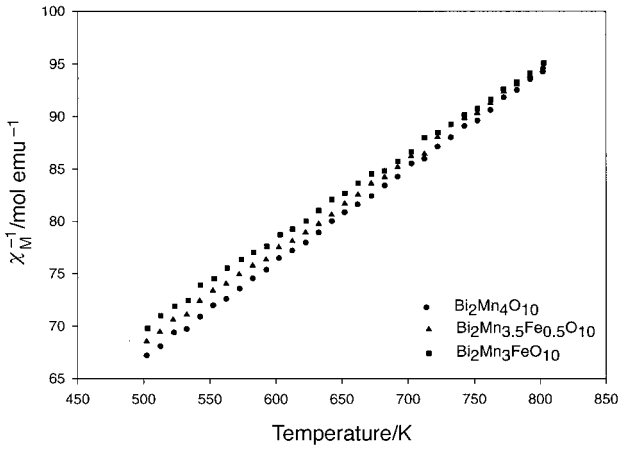

Fig. 3 Thermal dependence of the reciprocal molar magnetic susceptibility χ_M^{-1} for $Bi_2Mn_{4-x}Fe_xO_{10}$.

the proportion of Fe^{3+} in the octahedral sites increases significantly with x.

At this stage, a distribution of the Mn^{4+} and Mn^{3+} species between the two sites, O and P, can be proposed, based on size considerations, provided that the spin state of Fe^{3+} and Mn^{3+} can be confirmed. The $\chi^{-1}(T)$ curves, registered for $x=0$, 0.50 and 1 (Fig. 3) in the paramagnetic domain, can only be fitted with a high spin state for both Mn^{3+} and Fe^{3+}. Consequently the effective magnetic moment per metallic ion deduced from these curves increases regularly with x (Table 4) in agreement with the higher magnetic moment of Fe^{3+} in the $S=5/2$ state. Thus, considering that Mn^{3+} high spin and Fe^{3+} high spin have practically the same ionic radii in octahedral coordination according to Shannon and Prewitt,[14] we can explain the Mn(Fe)–O distances of the $Bi_2Mn_3FeO_{10}$ phase (Table 5) as follows: the significantly smaller M–O distances observed for the octahedral site (1.865–1.929 Å) compared to those in the pyramidal site (1.955–2.063 Å) show unambiguously that the octahedral site is preferentially occupied by Mn^{4+}, whereas Mn^{3+} lies on the pyramidal site. Consequently, the cationic distribution in this oxide can be formulated

Table 4 Effective magnetic moments observed for $Bi_2Mn_{4-x}Fe_xO_{10}$ ($0\leqslant x\leqslant 1$)

x	μ_{ex} (μ_B/ion M)
0	4.66
0.25	4.75
0.50	4.80
1	4.94

Table 5 Interatomic distances (Å) for $Bi_2Mn_{4-x}M_xO_{10}$ (M=Mn, Ti, Fe, Al)

M	x	Pyramid		Octahedron	
Mn	0	M–O(1)	1.880×2	M–O(2)	1.864×2
		M–O(2)	1.916×2	M–O(3)	1.820×2
		M–O(3)	2.175×1	M–O(4)	1.938×2
		<M–O>	1.953	<M–O>	1.874
Fe	1	M–O(1)	1.955×2	M–O(2)	1.865×2
		M–O(2)	1.980×2	M–O(3)	1.854×2
		M–O(3)	2.063×1	M–O(4)	1.929×2
		<M–O>	1.987	<M–O>	1.883
Ti	1	M–O(1)	1.921×2	M–O(2)	1.934×2
		M–O(2)	1.914×2	M–O(3)	1.890×2
		M–O(3)	2.120×1	M–O(4)	1.986×2
		<M–O>	1.958	<M–O>	1.937
Al	0.25	M–O(1)	1.849×2	M–O(2)	1.889×2
		M–O(2)	1.869×2	M–O(3)	1.872×2
		M–O(3)	2.077×1	M–O(4)	1.926×2
		<M–O>	1.903	<M–O>	1.896

Table 6 Atomic coordinates for $Bi_2Mn_3TiO_{10}$

Atom	Site	x	y	z	B/Å^2
Bi	4g	0.1617(2)	0.1645(1)	0	0.67(1)
Mn (P)	4h	0.4025(8)	0.3489(8)	0.5	0.75(1)
Mn, Ti (O)	4f	0.5	0	0.2573(10)	1.01(2)
O(1)	4e	0	0	0.2923(13)	1
O(2)	8i	0.3799(11)	0.1997(8)	0.2575(20)	1
O(3)	4h	0.1347(11)	0.4169(10)	0.5	1
O(4)	4g	0.1552(9)	0.4380(13)	0	1

as $Bi_2[Mn_{1.66}{}^{4+}Fe_{0.34}{}^{3+}]_O[Mn_{1.00}{}^{3+}Mn_{0.34}{}^{4+}Fe_{0.66}{}^{3+}]_PO_{10}$, showing that Mn^{4+} can also occupy partially the pyramidal site, in agreement with zur Loye's statement.[9] Comparison with the Mn–O distances in $Bi_2Mn_4O_{10}$ (Table 5) supports also this viewpoint. Moreover, one indeed observes that the distortion of the pyramid decreases from $Bi_2Mn_4O_{10}$ to $Bi_2Mn_3FeO_{10}$ as the Mn^{3+} cation is substituted by Mn^{4+} and Fe^{3+}; in contrast the substitution of Fe^{3+} for Mn^{4+} in the octahedral site does not influence significantly the distortion.

Substitutions by other cations: oxides $Bi_2Mn_{4-x}M_xO_{10}$ with M=Al, Ti

The substitution of titanium for manganese leads to a similar homogeneity range as for iron corresponding to $Bi_2Mn_{4-x}Ti_xO_{10}$ with $0\leqslant x\leqslant 1$, whereas in contrast a narrow range is obtained for $Bi_2Mn_{4-x}Al_xO_{10}$, with $0\leqslant x\leqslant 0.25$. The cell parameters of these phases are summarized in Table 1 and their coordinates in Tables 6 and 7, respectively. For the titanium phase, the metallic elements are distributed at random over the Mn sites; since titanium and manganese have close atomic numbers, it is not possible to determine their distribution from structural refinements. This is not the case for aluminium which has an atomic number half that of manganese. The structural refinement of $Bi_2Mn_{3.75}Al_{0.25}O_{10}$ shows indeed that Al^{3+} is located in the pyramidal site ($R_i=0.045$) rather than in the octahedral site $R_i=0.056$).

The magnetic susceptibility curves of these phases are given

Table 7 Atomic coordinates for $Bi_2Mn_{3.75}Al_{0.25}O_{10}$

Atom	Site	x	y	z	B/Å^2
Bi	4g	0.1584(1)	0.1659(2)	0	0.92(2)
Mn, Al (P)	4h	0.4091(9)	0.3477(8)	0.5	0.17(1)
Mn (O)	4f	0.5	0	0.2657(10)	0.75(2)
O(1)	4e	0	0	0.3052(14)	1
O(2)	8i	0.3869(11)	0.1976(9)	0.2652(14)	1
O(3)	4h	0.1470(14)	0.4211(12)	0.5	1
O(4)	4g	0.1451(13)	0.4518(13)	0	1

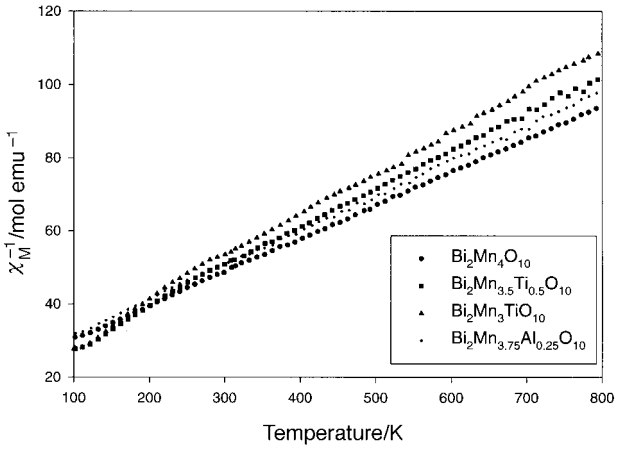

Fig. 4 Thermal dependence of χ_M^{-1} for $Bi_2Mn_{4-x}M_xO_{10}$ (M=Ti or Al).

Table 8 Experimental and calculated effective magnetic moments (μ_B/ion) for $Bi_2Mn_{4-x}Ti_xO_{10}$ ($0 \leqslant x \leqslant 1$) and $Bi_2Mn_{3.75}Al_{0.25}O_{10}$

	$Bi_2Mn_{4-x}Ti_xO_{10}$			$Bi_2Mn_{3.75}Al_{0.25}O_{10}$	
x	μ_{ex}	μ_{calc} with Ti^{3+}	μ_{calc} with Ti^{4+}	μ_{ex}	μ_{calc}
0 (this work)	4.66	—	—	—	—
0.25	4.55	4.26	4.33	4.56	4.24
0.50	4.30	4.11	4.20	—	—
1	4.13	3.77	3.97	—	—

in Fig. 4. The best fits in the paramagnetic domain were obtained with Mn^{3+} in high spin configuration, and for Ti^{4+}, Al^{3+} cations. The values of the effective magnetic moments, listed in Table 8, show that μ_{eff} is smaller for the titanium and aluminium substituted phases than for $Bi_2Mn_4O_{10}$, in agreement with the diamagnetic behavior of Ti^{4+} and Al^{3+}. The decrease of the magnetic susceptibility of the titanium phases as x increases confirms also the contribution of the diamagnetic character of Ti^{4+} to these properties.

The examination of the interatomic distances (Table 5) suggests that Ti^{4+} sit mainly in the octahedral sites and confirms pyramidal coordination for Al^{3+}.

Starting from the cationic distribution $Bi_2[Mn_2{}^{4+}]_O[Mn_2{}^{3+}]_PO_{10}$, proposed by Bertaut *et al.*,[7] a significant increase of the M–O distances in the octahedral sites should indeed be observed for $Bi_2[Mn^{4+}Ti^{4+}]_O[Mn^{3+}]_PO_{10}$ due to the larger size of Ti^{4+} compared to Mn^{4+}. In contrast, the average M–O distance in the pyramidal site should not vary significantly. The observations support strongly this viewpoint: one observes an average Mn^{4+}–O distance of 1.874 Å in the octahedral site for $Bi_2Mn_4O_{10}$ *cf.* 1.937 Å for $Bi_2Mn_3TiO_{10}$, whereas the average Mn^{3+}–O distance in the pyramidal site (1.953 Å for $Bi_2Mn_4O_{10}$) remains approximately constant (1.958 Å for $Bi_2Mn_3TiO_{10}$). Note also that the distortion of the pyramid has not decreased dramatically and in any case, less than in the case of iron substitution.

In the same way, the cationic distribution $Bi_2[Mn_2{}^{4+}]_O[Mn_{1.75}{}^{3+}Al_{0.25}{}^{3+}]_P O_{10}$, deduced from the XRD refinements is in perfect agreement with the evolution of the M–O distances. One indeed observes that the average M–O distance in the octahedra (1.896 Å) is close and even larger than that observed in $Bi_2Mn_4O_{10}$ (1.874 Å), whereas a significant decrease of the M–O distance in the pyramids (1.903 Å) is observed with respect to $Bi_2Mn_4O_{10}$ (1.953 Å), due to the substitution of Al^{3+} for Mn^{3+} in those sites.

Conclusion

We have prepared the substituted manganites $Bi_2Mn_{4-x}M_xO_{10}$ with $M = Fe^{3+}$, Ti^{4+}, Al^{3+}. For the iron substituted phases, combining X-ray powder diffraction, magnetic susceptibility measurements, ^{57}Fe Mössbauer spectroscopy and electric field gradient calculations permits us to confirm the high spin state of Mn^{3+} and Fe^{3+} and the preferential occupancy of Fe^{3+} in the square pyramidal site. It is also shown that this environment is preferentially occupied by Mn^{3+} rather than by Mn^{4+}.

The structural study of the titanium and aluminium substituted compounds shows that the Ti^{4+} and Al^{3+} sit in the octahedral and pyramidal sites of the $BiMn_4O_{10}$ structure respectively.

References

1 R. Mahendiran, R. Mahesh, A. K. Raychaudhuri and C. N. R. Rao, *Solid State Commun.*, 1995, **94**, 515.
2 J. Inoue and S. Maekawa, *Phys. Rev. Lett.*, 1995, **74**, 3407.
3 Y. Tokura, A. Urushibara, Y. Moritomo, T. Arima, A. Asamitsu, G. Kido and N. Furukawa, *J. Phys. Soc. Jpn.*, 1994, **63**, 3931.
4 V. Caignaert, A. Maignan and B. Raveau, *Solid State Commun.*, 1995, **95**, 357.
5 A. Maignan, Ch. Simon, V. Caignaert and B. Raveau, *Solid State Commun.*, 1995, **96**, 623.
6 *Colossal Magnetoresistance, Charge Ordering and Related Properties of Manganese Oxides*, ed. C. N. R. Rao and B. Raveau, World Scientific Publishing, Singapore, 1998.
7 E. F. Bertaut, G. Buisson and S. Quezel-Ambrunaz and G. Quezel, *Solid State Commun.*, 1967, **5**, 25.
8 E. F. Bertaut, G. Buisson and S. Quezel-Ambrunaz, *C.R. Acad. Sci., Paris*, 1964, **258**, 3025.
9 D. M. Giaquinta and H.-C. zur Loye, *J. Alloys Compds.*, 1992, **184**, 151.
10 J. Rodriguez-Carjaval, *Fullprof: a program for Rietveld Refinements and Pattern Matching Analysis*, *XVth Congress of Int. Union of Crystallography*, Toulouse, France, July 1990.
11 J. Teillet and F. Varret, unpublished MOSFIT program.
12 R. M. Sternheimer, *Phys. Rev.*, 1963, **130**, 1423.
13 P. Gütlich, R. Link and A. Trautwein, *Inorganic Chemistry Concepts.*, *Vol 3. Mössbauer spectroscopy and Transition Metal Chemistry*. Springer-Verlag, Berlin, 1978.
14 R. D. Shannon, *Acta Crystallogr., Sect. A*, 1976, **32**, 751.

Paper 8/08094A